Biochemical Pharmacology 83 (2012) 37–46

Contents lists available at SciVerse ScienceDirect

Biochemical Pharmacology

journal homepage: www.elsevier.com/locate/biochempharm

7β-Hydroxycholesterol-induced energy stress leads to sequential opposing signaling responses and to death of c6 glioblastoma cells

Ludovic Clarion [a,b], Mathilde Schindler [a], Jan de Weille [a], Karine Lolmède [c], Audrey Laroche-Clary [d], Emmanuelle Uro-Coste [c,e], Jacques Robert [d], Marcel Mersel [b,*], Norbert Bakalara [a,f,**]

[a] Institut des Neurosciences de Montpellier INSERM U-1051, 80 rue Augustin Fliche, 34295 Montpellier 05, France
[b] Beta Innov IRB Hôpital Saint Eloi, 80 rue Augustin Fliche, 34295 Montpellier 05, France
[c] Institut National de la Santé et de la Recherche Médicale (INSERM), U858, CHU Rangueil, BP 84225, 31432 Toulouse cedex 4, France
[d] Validation et identification de nouvelles cibles en oncologie U-916 Institut Bergonié, Centre Régional de Lutte Contre le Cancer, 229 Cours de l'Argonne, 33076 Bordeaux cedex, France
[e] Université Toulouse III Paul-Sabatier, Institut de Médecine Moléculaire de Rangueil, Equipe n°15, 1 Avenue Jean Poulhes, 31432 Toulouse Cedex 4, France
[f] Ecole Nationale Supérieure de Chimie de Montpellier 8, rue de l'Ecole Normale, 34296 Montpellier, France

ARTICLE INFO

Article history:
Received 24 August 2011
Accepted 21 September 2011
Available online 29 September 2011

Keywords:
Glioblastoma
Oxysterol
Lipid-raft
Energy stress
AMPK

ABSTRACT

7β-Hydroxycholesterol cytotoxicity has been shown *in vivo* and *in vitro* to be dependent on the accumulation of its esters. We show in our study, using a detergent-free raft preparation and LC/MS lipid content analysis, that membrane microdomains isolated from 7β-hydroxycholesterol-treated C6 cells have a reduced cholesterol: cholesterol ester ratio and accumulate 7keto-hydroxycholesterol, 7β-hydroxycholesterol and 7β-hydroxycholesterol esters. These modifications in lipid content are accompanied by a redistribution of flotillin-1 in the lipid rafts. Transient increases of AMPK phosphorylation and mitochondrial activity during the first 12 h of 7β-hydroxycholesterol treatment indicate that C6 cells undergo energy stress and increase oxidative phosphorylation. Even so, ATP levels are maintained during 15 h until glucose uptake decreases. The cell's answers to raft modifications and energy stress are sequential activations of different signaling pathways such as ERK, AMPK and PI3K/Akt. These pathways, known to be activated under energy stress conditions, are transiently activated at 6 h (ERK, AMPK) and 12 h (Akt) of treatment respectively suggesting a shift from cell survival to cell proliferation. The persistence of 7β-hydroxycholesterol-induced stress led after 24 h to P38 activation, loss of GSK3β activation and to cell death. Finally we demonstrate that the observed signaling responses depend on 7β-hydroxycholesterol esterification, confirming that esterification of 7β-hydroxycholesterol is essential for cytotoxicity.

1. Introduction

Gliomas are the most frequent brain tumor with an incidence of 5/100,000 inhabitants. These tumors are divided in two main categories: "primary high grade gliomas" (WHO grade IV), and "low grade gliomas" (WHO grade II glioma), with a constant growth and which ineluctably evolves to anaplasia (WHO grade III and then IV). Grade IV glioma or glioblastoma (GBM), is an infiltrating, vascularized and necrotizing multi-drug resistant tumor [1]. Typically, surgical resection, radiotherapy and/or chemotherapy (Temozolomide) are combined for treatment. However, mortality is still close to 100% within two years and the median survival of patients with GBM is around 1 year using classical treatments. As a consequence, new effective drugs to treat gliomas need to be found. In this context we studied the mode of action of the 7β-hydroxycholesterol (7βHC) which ester form was shown to inhibit growth of experimental rat C6 glioblastoma [2]. It has been reported that 7βHC is esterified by naturally occurring fatty acid in the C-3-OH position resulting in 7β-hydroxy-cholesteryl 3 ester (7βHC ester) and that its cytotoxicity is correlated with its degree of esterification [3,4]. Although highly toxic against transformed astrocyte cell lines [5] the 7βHC exhibits a poor toxicity against primary culture of rat and mouse astrocytes [6].

Oxysterols are 27-carbon derivatives of cholesterol or by-products of cholesterol biosynthesis [7]. They are either formed by

Abbreviations: 22HC, 22-hydroxycholesterol; 25HC, 25-hydroxycholesterol; 7kCH, 7keto-cholesterol; CH, cholesterol; 7βHC, 7β-hydroxycholesterol; 7βHC ester, 7β-hydroxy-cholesteryl 3 ester; CH ester, cholesterol ester; PL, phospholipid; cav-1, caveolin-1; flot-1, flotillin-1; ACAT, acyl-CoA:cholesterol acyltransferase; THF, tetrahydrofurane.

* Corresponding author.
** Corresponding author at: Ecole Nationale Supérieure de Chimie de Montpellier 8, rue de l'Ecole Normale, 34296 Montpellier, France. Tel.: +33 4 99636067; fax: +33 4 99636020.
E-mail addresses: m.mersel@beta-innov.com (M. Mersel), norbert.bakalara@enscm.fr (N. Bakalara).

0006-2952/$ – see front matter © 2011 Elsevier Inc. All rights reserved.
doi:10.1016/j.bcp.2011.09.022

cholesterol oxidation catalyzed by cytochrome P450 enzymes, or by non enzymatic auto-oxidation processes [8]. If 27-, 24-, 7α and to a lesser extent 22- and 25-hydroxycholesterol (22HC, 25HC) are enzymatically synthesized 7-ketocholesterol (7kCH), 7βHC and 5β, 6β-epoxycholesterol are non enzymatically formed. Because oxysterol are found in the human diet [9], in tissues as well as in blood circulation a new interest has been given to the study of their biological roles [8] which have been largely documented for more than thirty years [10]. Their implications in morphogenesis [11], retina degenerative processes [12], atherosclerosis [13] and cholesterol biosynthesis regulation have been well reported. One of the most exciting biological properties of oxysterols is their action against tumoral cells [14]. Among them, 7βHC, isolated from the traditional Chinese anticancer drug Bombyx cum Botryte [15], has been thoroughly investigated because of its marked cytotoxic effect on hepatocarcinoma [16], lymphomas [17] and spontaneously transformed astrocytes [18]. More recently, *in vitro* assays have shown that 7βHC-induced apoptosis in colon adenocarcinoma [19], in head and neck squamous carcinoma [20] and in lung carcinoma [21] cell lines. However, despite all these physiological observations about their biological involvements little is known about their antiproliferative mode of action.

Several authors reported that, after treatment with 7βHC, tumor cells die by apoptosis due to cytochrome c release from mitochondria and caspase 3 activation [22–25]. This is remarkable given that tumor cells hardly solicit mitochondria as they rely mostly on glycolysis for their energy requirements [26,27]. The objective of this study is to determine the early cellular and molecular events induced by 7βHC leading to cell death, using the C6 glioblastoma cell model. In this paper we show that 7βHC esters accumulate in lipid rafts during the first 24 h of 7βHC treatment. The cholesterol (CH):cholesterol ester (CH ester) ratio as well as flotillin-1 (flot-1) distribution in lipid rafts are modified. These membrane modifications induced an energy stress as witnessed by increase in both AMPK phosphorylation and glucose oxidation 6–7 h after 7βHC addition. Next, the ERK, PI3K/Akt signaling pathways are sequentially activated in response to this stress. Finally after 24 h, activation of the P38 signaling pathway leads to cell death.

2. Materials and methods

2.1. Cell culture

The C6 glioma cell line, originally cloned from a *N*-nitrosomethylurea induced glioma (61), was obtained from the American Type Culture Collection and tested in 2008 by immuno-fluorescence for GFAP expression. Briefly, passages were obtained by digestion with 0.05% trypsin (from bovine pancreas, Sigma) supplemented with EDTA (Sigma), and filtered through 0.2 μm. Cells were seeded on 75 cm^2 Corning cell culture flasks at a density of 20,000 cells/mL in MH5V [70% MEM (Gibco), 30% HBSS (Gibco) and 5% heat inactivated FBS (Invitrogene)] with 2.5 μg/mL of Fungizone (Gibco) and 5 μg/mL of Cyprofloxacine (Euromedex) and maintained at 37 °C under humidified 5% CO_2–95% air atmosphere. 7βHC was solubilized in absolute EtOH (at a stock concentration of 30 mM) and treatments were carried out 24 h after seeding. Cells were treated with absolute EtOH as controls. Tetracaine was solubilized in EtOH/water 1:3 (final concentration 30 mM) and treatments were carried out in the same conditions as for 7βHC.

2.2. Immunocytochemistry and microscopy

C6 cells (20,000) were seeded in 24-well plates (Nunc, 9.6 cm^2/well) containing poly-D-lysine (Sigma–Aldrich)-coated glass coverslips (diam. 12 mm). After 24 h of culture, cells were treated with 30 μM of 7βHC for 24 and 48 h. Cells were then washed twice with PBS (Sigma–Aldrich), fixed and permeabilized with methanol at −20 °C for 10 min and incubated with anti-caveolin-1 antibody (1:100; Abcam) overnight at 4 °C followed by incubation with goat anti-rabbit antibody conjugated to Alexa 488 (1:1500, Jackson) for 1 h at room temperature and with anti-flotillin-1 (1:200, BD Biosciences) followed by goat anti-mouse Cy3 antibody (1:1500, Jackson). All antibodies were incubated in PBS supplemented with 1% BSA (Sigma), 5 μg/mL Hoechst 33258 (Sigma–Aldrich) and 0.05% Azide (Sigma–Aldrich). Dako mounting medium was used for all observations. Image bit depth was 16 bits and exposure time was 500 ms for caveolin and 300 ms for flotillin. Space resolution of all images was 150 ppi. Fluorescence microscopy was performed with a Zeiss AxioimagerZ1.

2.3. Cell harvesting and lysis

Cell resuspension and lysis were carried out at 4 °C. Cell lysates were prepared from C6 cells treated either with EtOH as control or with 10 or 30 μM of 7βHC for 24 and 48 h. Having reached 70% of confluence, cells were washed twice in cold PBS and incubated for 10 min at 4 °C under gentle shaking with 1 mL of cold lysis buffer [Cell signaling lysis buffer 10× (200 mM Tris–HCl (pH 7.5), 1.5 M NaCl, 10 mM EGTA, 10 mM EDTA, 10% Triton, 25 mM sodium pyrophosphate, 10 mM β-glycerophosphate, 10 mM Na_3VO_4 (Sigma–Aldrich), 10 μg/mL leupeptin and complete protease inhibitors or phosphatase inhibitor (Roche)]. Cells were harvested using a scraper (Nunc). Cell suspension was centrifuged for 5 min at 10,000 × *g* at 4 °C (partition of fragments membrane and DNA). The supernatant was stored at −80 °C.

2.4. Glucose uptake

C6 cells were cultured until they reached 50% confluence. Cells were subsequently treated with 20 μM of 7βHC for the times indicated. Cells were then incubated for 30 min in DMEM devoid of glucose, but containing 2 mM of deoxyglucose and 2 μM of C^{14}-deoxyglucose (2.13 GBq/mmol), washed twice with PBS. Deoxyglucose uptake was measured using a scintillation counter (Perkin-Elmer). Vehicle (0.05% ethanol) was without effect on cell growth or deoxyglucose uptake. The Serf software (http://www.bram.org/serf/CellsAndMaps.php) was used for the statistical analysis (ANOVA).

2.5. Mitochondrial activity (JC1 fluorescence) [28]

Mitochondrial activity was estimated using the bi-fluorescent dye JC1 (Sigma France). Cells were incubated for 2 h in the presence of 3 μM JC1 and then fixed with 4% formaldehyde. Red and green image pairs were taken with an Olympus X70 fluorescence microscope (Olympus, France) and the ratio of red over green fluorescence was determined for each separate cell in the image pairs using Serf software (http://www.bram.org/serf/CellsAndMaps.php) (ANOVA).

2.6. ATP content measurements [29]

C6 cells were grown in 25 cm^2 flasks, treated with 20 μM of 7βHC for the indicated times, harvested using 0.1% trypsin digestion for 5 min, centrifuged and kept at −20 °C. Cells subsequently thawed on ice and lysed by 100 μL of a 1% triton PBS solution. 90 μL were used to determine protein content and the remaining 10 μL were rapidly mixed with adequate amounts of luceferin and luciferase (Sigma, France) and emitted photons were counted using a Wallac 1450 microbeta counter (Perkin-Elmer, France). The Serf software

(http://www.bram.org/serf/CellsAndMaps.php) was used for the statistical analysis (ANOVA).

2.7. Cell proliferation and MTT viability assay test

C6 cells were seeded in 96-well plates at a density of 3000 cells/well. After 24 h, cells were treated with 10 or 30 μM of 7βHC and controls were treated with EtOH. Incorporation and reduction of Thiazolyl Blue Tetrazolium Bromide (0.1 mg/mL in MH5 V, Sigma–Aldrich) was carried out at various times following treatment and measured at 570 nm in DMSO with a microplate reader (model 550, Bio-Rad) [30].

2.8. Antibodies and chemicals

Antibodies anti Akt (pan), p-Akt (Thr308), p-AMPKα (Thr172), AMPKα, P38, p-P38 (Thr308/Tyr182), p-P38 (Thr180/Tyr182), p-p44/42 (Erk1/2) (Thr202/Tyr204), p44/42(Erk1/2), GSK3β, p-GSK3β (Ser9), were purchased from Cell Signaling Technology and used at a dilution of 1:1000 for western blotting. As none or very little expression of GSK3α was detected in our C6 cell model, we have only considered GSK3β activity. 7βHC (H6891, ≥95%) and tetracaine (T7383, ≥98%) were purchased from Sigma–Aldrich.

2.9. Western blotting

Protein concentrations were determined by BCA assay (Pierce), verified by coomassie blue staining of SDS–PAGE and calibrated against β-actin. Total kinase detection was performed loading 3 μg of total proteins and the corresponding phosphorylated kinase was detected loading 30 μg of total proteins. Cell lysates denatured in Laemmli buffer 3× containing 150 mM DTT at 95 °C for 5 min were resolved by SDS–PAGE 10% acrylamide, transferred for 1 h at 15 V to PVDF membranes (hybond, Amersham) by Trans-Blot-SemiDry-Transfer Cell (Bio-Rad). Membranes were then blocked for 60 min at 20 °C with TBS (20 mM Tris–HCl, 270 mM NaCl, pH = 7.5) containing 0.1% Tween-20 (Bio-Rad) and 5% (w/v) fat-free milk and incubated overnight at 4 °C with primary antibodies, diluted in the blocking solution. Revelation was performed by using horseradish peroxidase conjugated secondary antibodies (Jackson) at a dilution of 1:10,000 in blocking buffer, and the peroxidase/chemiluminescence method (Immobilon ECL western blotting system; Millipore) using BioMax films (Kodak). Quantifications were normalized with respect to total unphosphorylated protein.

2.10. Raft isolation and determination of 7βHC esterification [31]

Cells were rinsed twice with cold PBS and scraped off in 1 mL of buffer containing 20 mM Tris–HCl, 250 mM sucrose, pH 7.8, 1 mM $CaCl_2$ and 1 mM $MgCl_2$. After the addition of 4 mL of fresh medium (MH5 V), cells were centrifuged at 250 × *g* for 2 min. The supernatant was removed and the pellet was resuspended, after 20 up- and down-pipettings through a 22G needle, with 210 μL of buffer containing 20 mM Tris–HCl, 250 mM sucrose, pH 7.8, 1 mM $CaCl_2$, 1 mM $MgCl_2$ and complete protease inhibitors (Roche). Lysates were then centrifuged at 4 °C at 10,000 × *g* for 10 min and 1 volume of 50% OptiPrep™ (Sigma) solution was added to the supernatant giving a 25% OptiPrep™ sample. The OptiPrep™ solutions were prepared in a buffer containing 20 mM Tris–HCl, 250 mM sucrose, pH 7.8 and samples were loaded on an OptiPrep™ step gradient (5%, 10%, 15%, 20%). The gradient was centrifuged for 90 min at 52,000 × *g* and 4 °C (TLS-500 rotor, UltraMax, Beckman). The gradient was recovered in 10 fractions of 210 μL each. 10 μg of proteins were resolved by SDS–PAGE. Anti-cav-1 (antibody dilution: 1 μg/mL, Abcam), anti-flot-1 (antibody dilution 1:500, BD Biosciences) and anti-transferrin receptor (1:100, Abcam) antibodies were used to identify by western blotting fractions containing the raft microdomains.

2.11. Dialysis of raft fraction containing OptiPrep™

Pierce cassettes were used to dialyze each fraction (10K MWCO, 3–12 mL). OptiPrep™ removal was followed by an optical density measurement using a spectrometer (Shimadzu) at 490 nm. Pooled fractions were dialyzed against 4 L of Tris–HCl, pH 7.8 buffer without sucrose at 4 °C for 24 h under stirring. Buffer was renewed every 6 h during 24 h. For all samples, optical density and protein concentration were determined.

2.12. Extraction and saponification of raft fractions

According to Folch's method [32], extraction of cholesterol derivatives was achieved in a chloroform/methanol mixture (2:1, 19 vol. of aqueous layer) for 2 h at room temperature. After addition of 0.2 vol. of ultrapure water two phases were observed. After decantation, the organic layer was dried and evaporated under reduced pressure. The oily residue was dissolved in a small volume of THF for injection in liquid chromatography (LC)/mass spectroscopy (MS). Next, saponification was carried out in 1 mL of tetrahydrofurane (THF), with 1 mL of 2 M methanolic solution of NaOH (NaOH 1 M final) for 24 h at room temperature. The mixture was diluted in 20 mL of chloroform and after the addition of 5 mL of water vigorously shaken and left 2 h at room temperature before decantation. The organic layer was dried and evaporated under reduced pressure. The oily residue was re-dissolved in a small volume of THF for LC–MS injection. LC was performed on a Waters 2790 with a BDS Hypersil CI8 column (Thermo, 50 mm × 2.1 mm, 3 μm), eluted with acetonitrile/water containing 0.1% trifluoroacetic acid. Mass detection was carried out by positive electrospray, on a Waters Micromass QTOF apparatus.

3. Results

3.1. Alteration of sterol content in lipid rafts after 24 h of 7βHC treatment

Plasma membrane cholesterol and phospholipid analysis have shown that 20 μM of 7βHC does not affect the ratio CH:phospholipids (CH/PL) in normal cells; in contrast, plasma membranes of transformed cells treated with 20 μM of 7βHC displayed a significantly decreased CH/PL ratio without affecting membrane fluidity [6]. This decrease in the CH/PL ratio coincided with accumulation of 7βHC-esters due to the activation of acyl-CoA:cholesterol acyltransferase (ACAT) by 7βHC [4]. These data prompted us to evaluate the presence of 7βHC and its ester forms in the plasma membrane and more precisely in lipid rafts (Fig. 1). Although rafts are commonly isolated using detergents, several observations raised concerns that extraction with detergent might be generating clusters of raft lipids and proteins that do not exist in the intact cell [33]. To avoid this we used a simplified detergent-free method for the preparation of lipid rafts [31]. We first analyzed the sterol contents in the selected fractions corresponding to lipid-raft (Fig. 2). OptiPrep™ gradient fractions 3 and 4 were pooled for sterol extraction and analysis. In order to identify various sterols we have chosen a liquid chromatographic separation method, thus avoiding a derivatisation step that would it make difficult to identify sterols by mass spectroscopy [34]. Commercial CH, 7kCH, 7βHC, 22-HC and 25-HC were used as markers for the identification of sterols in the raft fraction. Fig. 1A and C shows that CH and 7kCH are found in both control and treated samples. Interestingly, free CH represents 75% of total sterols in control, but only 2% in the treated samples. This data is in agreement with the reported

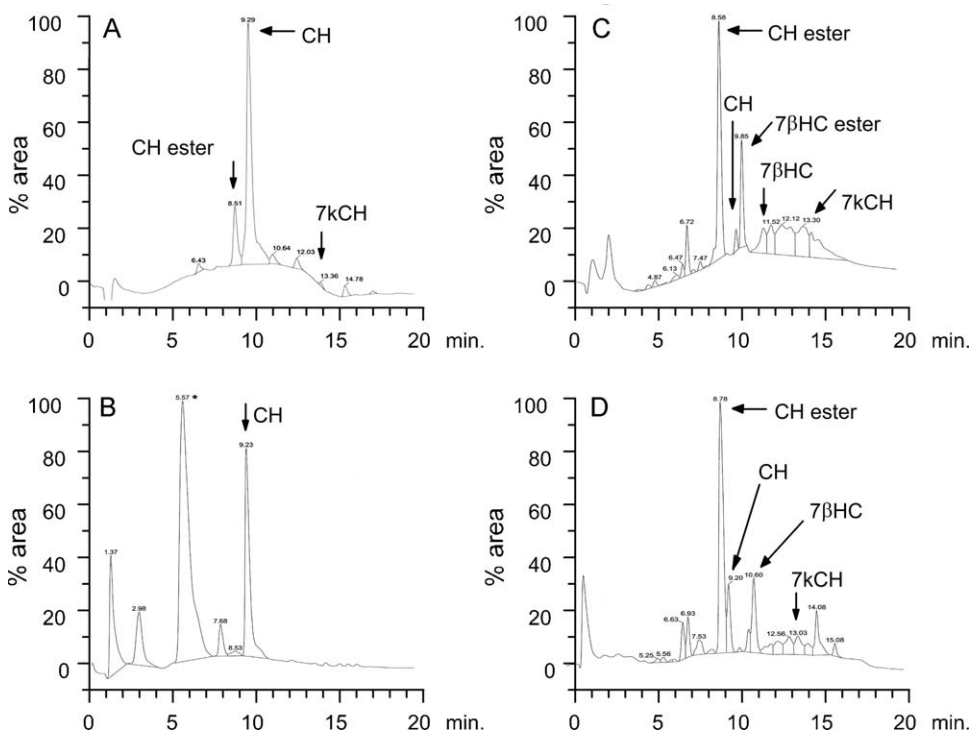

Fig. 1. 7βHC modifies the C6 sterol content of lipid raft microdomains. OptiPrep™ gradient fractions 3 and 4 of non treated cells and cells treated for 24 h with 7βHC were pooled. Sterols were extracted and separated by liquid chromatography and characterized by mass spectroscopy. (A–C) Liquid chromatography profile of extracted sterols from non treated cells (A) and 30 μM 7βHC-treated cells (C). (B–D) Liquid chromatography profile of extracted and saponified sterols from non treated cells (B) and 30 μM 7βHC-treated cells (D). (B) The peak at 5.57 min corresponds to cholesterol-O-methyl formed during the saponification process. (D) The peak at 8.78 min denotes that all the cholesteryl esters have not been totally saponified. Peaks were analyzed by mass spectroscopy and sterol identification was carried out using standard commercial CH (Sigma–Aldrich), cholesteryl ester (CH ester) (own synthesis according to Bochelen et al. [68]), 7kCH (Sigma–Aldrich), and 7βHC (Sigma–Aldrich).

observation about the decrease of the CH/PL ratio in transformed astrocytes [6]. Moreover, 7kCH recovered at 0.63% in the control represents 11% of total sterols in treated samples. The same liquid chromatography and mass spectrometry analysis was carried out after saponification (Fig. 1B and D). That treatment does not modify the amount of free CH in the control (77% of total sterol) indicating that in non-treated cells only a small percentage of CH is esterified (Fig. 1B). After saponification, free CH represents 46.6% of total sterols in 7βHC-treated cells. This result indicates that in treated cells most of the CH is esterified. 7βHC is only detected in treated

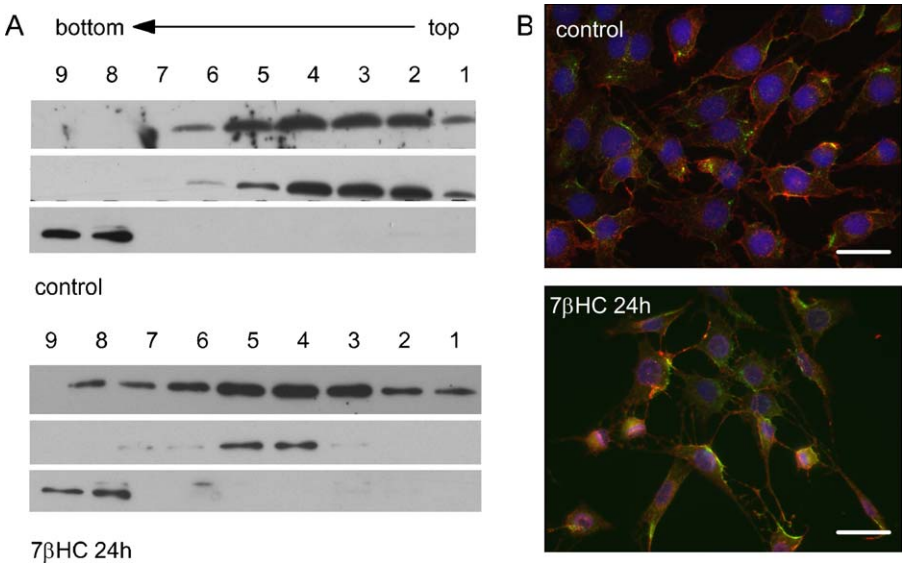

Fig. 2. 7βHC induces cav-1 and flot-1 redistribution in C6 lipid raft fractions. (A) C6 cell lysates from non treated cells (CT) and cells treated for 24 h with 30 μM of 7βHC were separated on an OptiPrep™ step gradient (5–25%). Ten fractions were collected from the gradient and the protein content quantified. 10 μg of proteins of the first 9 fractions were separated and immunoblotted using anti-cav-1, anti-flot-1 and anti transferrin receptor (Tfr-R) antibodies. These antibodies were tested against the same membrane which has been precut before incubation. (B) Immunofluorescence assays using anti-cav-1 (green) and anti-flot-1 (red) antibodies. Time exposures were of 300 and 500 ms cav-1 and flot-1 respectively. Nuclei were stained with Hoechst (blue) time exposure 20 ms. Scale bar, 20 μM.

cells (Fig. 1C and D). From the saponification experiment we can conclude that 70% of 7βHC in lipid rafts is esterified. These results confirm the previous observation that 7βHC not only stimulates its own esterification but also those of other sterols [4].

3.2. Redistribution of flot-1 in lipid rafts after 24 h of 7βHC treatment

A variety of proteins have been shown to be selectively enriched in lipid rafts. They include structural proteins such as flot-1 and cav-1 as well as signaling proteins [35,36]. As lipid raft sterol content changed with 7βHC treatment, we searched for changes in cav-1 and flot-1 distributions in the different OptiPrep™ fractions. The western blot analysis shows the distribution of cav-1 and flot-1 raft markers across the OptiPrep™ density gradient (Fig. 2A). In control cells, Flot-1 was principally found in fractions 2–4 while cav-1 rafts were found in fractions 2–5. The transferrin receptor, used as a plasma membrane marker, was found in fractions 8 and 9. The immunofluorescence study (Fig. 2B) shows that flot-1 has a punctuated distribution on the plasma membrane and is also located around the nucleus. Cav-1 is also discontinuously distributed at the plasma membrane and around the nucleus. However, flot-1 and cav-1 do not completely colocalize. Flot-1 is present in membrane microdomains in which cav-1 is absent (Fig. 2B). Taken together the gradient and the immunofluorescence analysis suggest that cav-1 and flot-1 localize within different lipid raft populations. After 24 h of 30 μM 7βHC treatment, lipid rafts were isolated according to the same procedure as above. Western blot analysis shows a different distribution of flot-1 across the gradient fractions. Flot-1 shifted from fractions 2–4 to fractions 4 and 5 (Fig. 2A). Although, cav-1 appears to be more spread over the gradient fractions, the global distribution of this raft marker was not modified. The flot-1 redistribution is confirmed by the immunofluorescence micrographs presented in Fig. 2B. Most of the punctuated distribution of flot-1 on the plasma membrane is lost. However the perinuclear distribution is conserved. As for cav-1, its discontinuous distribution on the plasma membrane is conserved. These results suggest that after 7βHC treatment, cav-1 is still present in lipid rafts whereas flot-1 diminished or even disappeared in these structures.

3.3. Lipid raft sterol and flot-1 redistributions are associated with energy stress and cell death

It has been previously shown that 30 μM of 7βHC induces cell death after 48 h [19,37]. In order to identify early molecular and cellular events leading to cell death, a MTT cell viability test was carried out during 48 h following 10 and 30 μM of 7βHC treatment. Fig. 3A shows that the antiproliferative effect of 30 μM of 7βHC appears after 6 h of treatment. Progress of necrosis and apoptosis were estimated using propidium iodide and Annexin V-FITC. Our data indicate that following initial necrosis at 12 h other cells die by apoptosis after 24 h (not shown). As a consequence the further analyses were carried out using these (6, 12, 24 h) time points.

Both sterol content and flot-1 expression/distribution have been reported to play a role in the cell energy metabolism [38] and in cell growth regulation [39,40]. Therefore in a next step we addressed the question whether accumulation of 7βHC and its ester forms in lipid rafts and flot-1 redistribution could generate cellular stress and cell signaling modifications leading to cell growth inhibition. The role of AMPK in regulating cellular energy load places this enzyme at a central check point in maintaining energy homeostasis [41]. We measured whether AMPK phosphorylation levels were modified before cell growth inhibition (6 h), and cell apoptosis (12 h) and once apoptosis is detected (24 h). Fig. 3B shows that using 30 μM 7βHC, AMPK phosphorylation

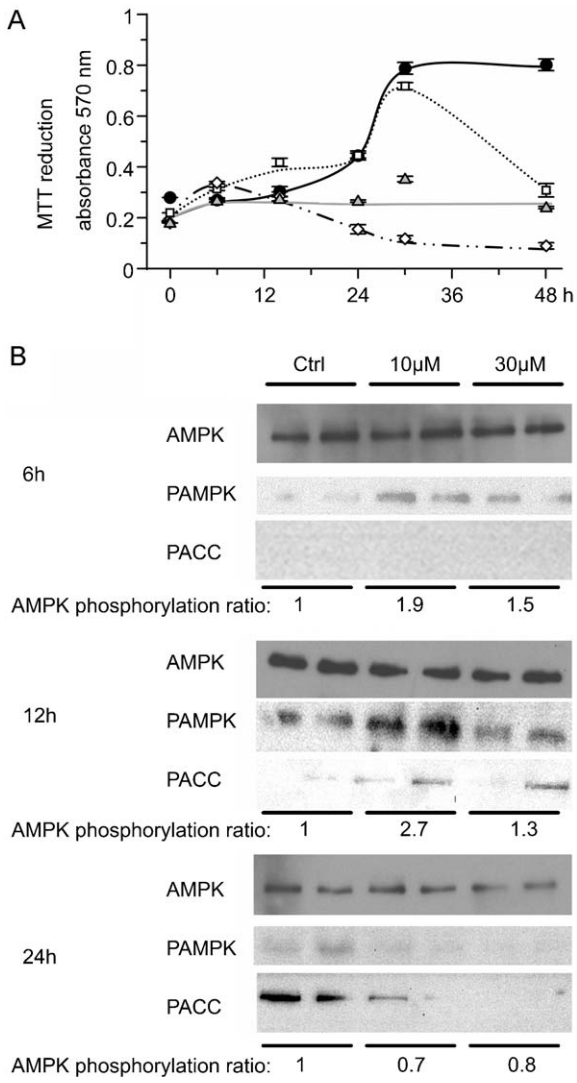

Fig. 3. 7βHC induces an energy stress and cell death in a dose- and time-dependent manner. (A) Growth rate of non treated cells (dark line) and 10 μM 7βHC- (dotted line), 30 μM 7βHC- (dashed line) and 1 μM staurosporine- (light grey) treated C6 cells. Cell proliferation was estimated by MTT reduction (means ± SD; $n = 5$). (B) C6 cells were treated either with vehicle (CT) or with 10 or 30 μM of 7βHC for 6, 12 and 24 h. Protein samples were quantified, calibrated against β-actin and immunoblotted with anti-AMPK, anti-phosphoAMPK (AMPKP). AMPK phosphorylation level detection was performed using the chemiDoc XRS system from BIORAD and Imagelab software.

increases transiently with a maximum at 6 h suggesting that C6 cells undergo an energetic stress similar to glucose deprivation. The amplitude and the period of activation of AMPK were increased when 7βHC was used at 10 μM instead of 30 μM (Fig. 3B), concomitantly the toxic effect of 7βHC at 10 μM was delayed until 30 h (Fig. 3A).

Once activated AMPK has been proposed to phosphorylate a number of targets involved in ATP production [42]. The acetyl-CoA carboxylase (ACC) represents one of these AMPK targets [43]. We therefore estimate in a next step whether or not AMPK activation was followed by ACC phosphorylation. Fig. 3B shows that ACC phosphorylation was coupled with AMPK phosphorylation.

In a next step a link between the energetic stress and glucose uptake was investigated. Glucose uptake was measured during the first 24 h of treatment but at 20 μM in order to still have the antiproliferative effect during that period (data not shown) but reducing secondary effects due to the cell apoptosis by itself at 24 h. Fig. 4A indicates that glucose uptake by 7βHC-treated C6 cells is reduced by 30 and 80% at 8 and 18 h of treatment. However

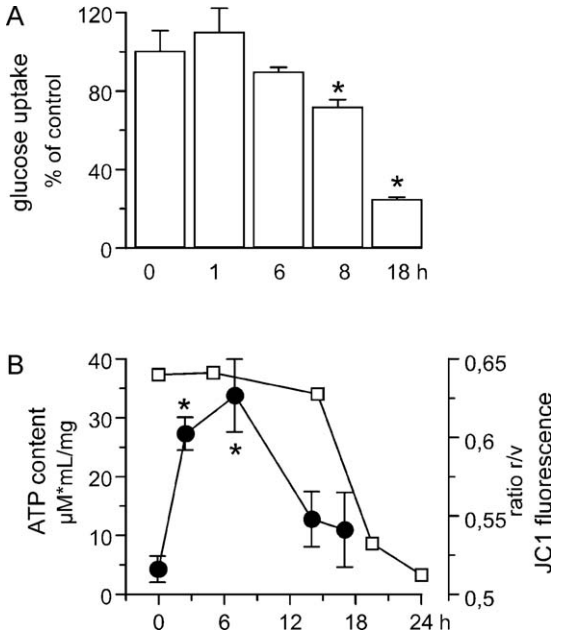

Fig. 4. 7βHC induces an energy stress and cell death in a dose- and time-dependent manner. (A) Deoxyglucose uptake into 7βHC-treated C6 cells. C6 cells were exposed to 20 μM of 7βHC for the indicated times. Deoxyglucose uptake as a percentage of control uptake is significantly lower with respect to control (t = 0 h) at 8 and 18 h. (B) C6 cells were treated with 20 μM of 7βHC and the evolution of ATP content (circles) and mitochondrial activity (squares) was monitored. ATP levels were quantified by a luciferase assay. Starlets indicate $p < 0.05$.

ATP levels remain constant for 15 h which corroborates with an up-regulation the mitochondrial activity reaching a maximum at 7 h (Fig. 4B). A drastic diminution of intracellular ATP follows (Fig. 4B) both the arrest of mitochondrial activation (Fig. 4B) and the decrease in glucose uptake (Fig. 4A). Taken together, these data suggest that AMPK activation is the cell's initial answer to protect itself against the stress brought about by 7βHC but it fails.

3.4. 7βHC treatment induces Erk signaling decrease, transient PI3K/Akt activation and P38 activation

We hypothesized that the AMPK activation described above was the initial cell's answer to 7βHC application to protect itself against energy stress. ERK, a canonical signaling pathway involved in cell survival, has been shown to be activated by glucose [44,45]. The PI3K/Akt signaling pathway is known to be implied in glucose metabolism regulation as well [46]. Therefore in a next step we studied the activation state of these signaling pathways following the energetic stress caused by the 7βHC treatment.

In accordance with the kinetic studies of Figs. 3 and 4, signaling studies were performed after 6, 12 and 24 h of 7βHC treatment. Fig. 5 shows a transient activation of ERK (6 fold) during the first 6 h of 30 μM 7βHC treatment. This pathway is partly inhibited at 12 h, and completely inhibited at 24 h of treatment with 7βHC. Although phosphorylation of Akt on Ser 473 stayed unmodified by 7βHC treatment (data not shown), Thr 308 phosphorylation increased as soon as 6 h with a maximum at 12 h (7 fold at 30 μM 7βHC) (Fig. 5). We also show in Fig. 5 that phosphorylation of GSK3β corroborates with Akt activation as we observed that at 12 h of treatment both Akt phosphorylation on Thr308 (7 fold) and GSK3 phosphorylation on Ser9 (1.7 fold) are increased. Phosphorylation of GSK3α was not increased (data not shown).

P38 on its turn has been reported to participate with AMPK in the stimulation of glucose uptake [47,48]. We therefore analyzed the effect of 7βHC on P38 phosphorylation. Fig. 5 shows that P38 starts to be activated after 12 h and reached maximum activation at 24 h (53 fold). At the same time, less GSK3β becomes phosphorylated and therefore more GSK3β is active.

3.5. Modulation of cell signaling and modification of raft structure depend on 7βHC esterification

Because 7βHC is esterified in the endoplasmic reticulum by ACAT on C-3-OH [3], we investigated the effect of ACAT inhibition by tetracaine on flot-1 and cav-1 distributions as well as on P38, Akt, and GSK3 phosphorylation states.

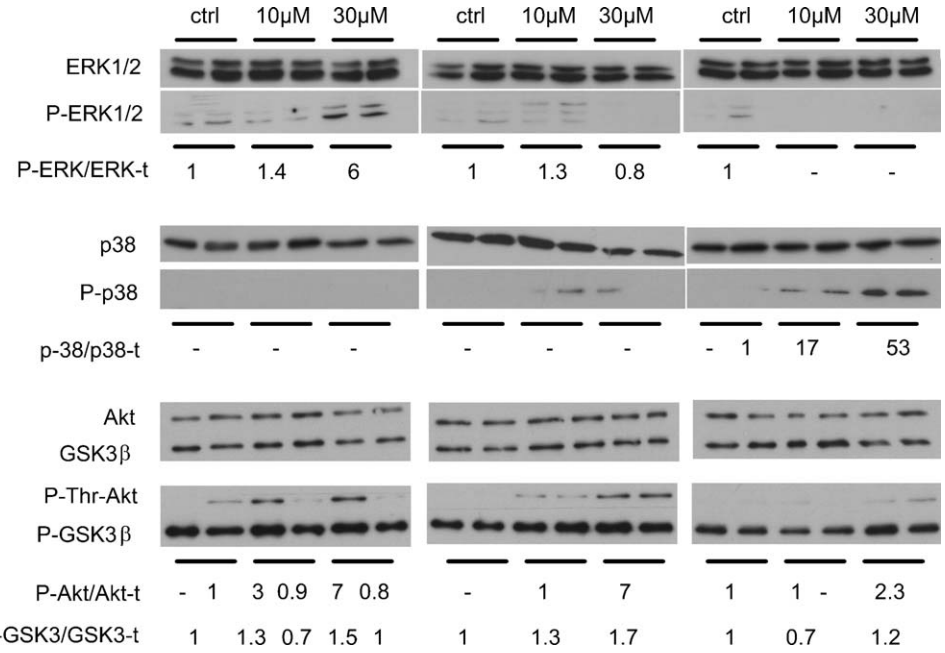

Fig. 5. 7βHC modulates ERK, Akt, GSK3 and P38 signaling in a dose- and time-dependent manner. C6 cells were treated either with vehicle (CT) or with 10 or 30 μM of 7βHC for 6, 12 and 24 h. Protein samples were quantified and immunoblotted with anti-ERK 1/2, anti-Akt, anti-P38, anti-phosphoERK (p-Erk 1/2), anti-phosphoAkt (pThr-Akt), anti-phosphoP38 (p-P38), antiGSK3β and anti-phosphoGSK3β (p-GSK3β) antibodies. The levels of phosphorylation (Qt) were estimated using the Image J software on different autoradiography exposures.

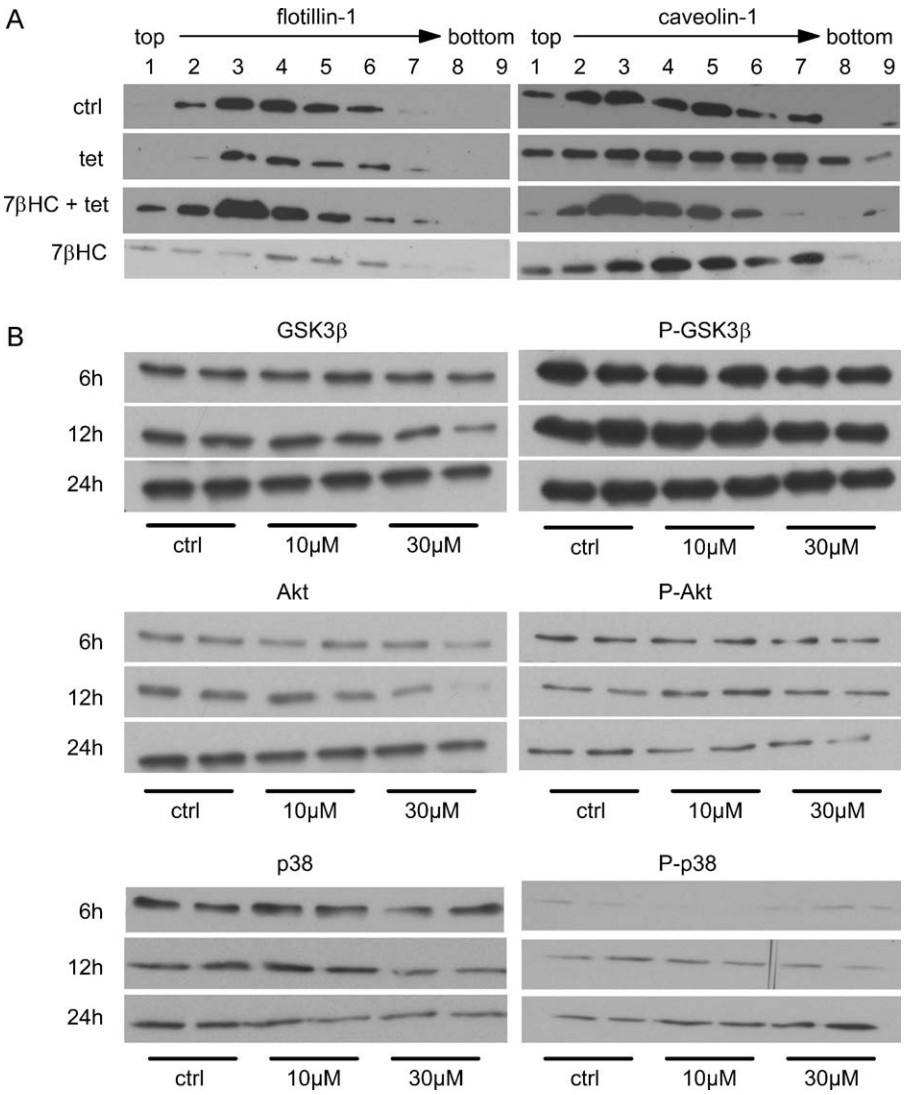

Fig. 6. The effect of 7βHC on raft structure and signaling is inhibited by tetracaine. C6 cells were treated either with vehicle (CT), tetracaine alone (CT-tet), 7βHC alone (7βHC) or simultaneously with tetracaine and 7βHC (7β-tet) for 6, 12 and 24 h. (A) cav-1 and flot-1 in the different OptiPrep™ gradient fractions were analyzed by immunoblotting of C6 cell lysates (10 μg) with anti-cav-1 and anti-flot-1 antibodies. (B) Cells were grown in the presence of 30 μM tetracaine and either treated or not with 10 or 30 μM of 7βHC. Protein samples were calibrated against β-actin and immunoblotted with anti-GSK3β, anti-Akt, anti-P38, anti-phosphoGsk3β, anti-phosphoAkt, anti-phosphoP38 antibodies.

Fig. 6A shows that the change in flot-1 distribution observed in 7βHC-treated C6 cells (Fig. 2A), does not occur if oxysterol esterification is blocked by 30 μM of tetracaine. Similarly, P38 and Akt phosphorylation are not affected by 7βHC if esterification is inhibited. In addition, GSK3β phosphorylation, which increases by 7βHC treatment, is not modified if 7βHC esterification is blocked by 30 μM of tetracaine (Fig. 6B).

4. Discussion

We demonstrated the existence of different types of membrane micro-domains in the C6 cells. This result confirms the observation that flot-1 is found in triton-insoluble/cholesterol-enriched domains in cells that do not contain cav-1 [49]. Next we have shown that addition of 30 μM of 7βHC to C6 GBM cells is characterized by the presence of oxidized cholesterols such as 7kHC, 7βHC and esters of cholesterols in lipid rafts. We measured the accumulation of these sterols only after 24 h of treatment. Unfortunately the sterol detection technique we used did not allow us to estimate the presence and amount of these sterols at earlier times, but it may reasonably be supposed that esterification starts right from the beginning of treatment with 7βHC, building up over time. Sterol transport through the cytosol to caveolae is known to be carried out by a vesicle-independent mechanism [48] involving cav-1. Cav-1 is part of a cytosolic HSP-immunophilin chaperone complex binding to and translocating newly synthesized cholesterol to caveolar membranes [48]. It has also been reported that Cav-1 binds cholesterol [50] and oxysterols such as 7kHC [51] and cholesteryl ester [52]. 7βHC and its ester form could therefore compete with other sterols for binding to cav-1 therewith modifying cav-1 sterol transport capacities. We observed a decrease of the cholesterol: cholesterol ester ratio and an increase of 7kHC, 7βHC and 7βHC ester in membrane micro-domains (Fig. 1). These findings agree with the observation that, in mouse embryonic fibroblasts (MEF), lipid microdomain homeostasis depends on cav-1 expression [53]. In conclusion, these data strengthen the hypothesis that cav-1, and more generally lipid rafts, are therapeutic targets for the treatment of certain cancers [54].

Although tetracaine does not suppress 7βHC cytotoxicity we observed that tetracaine antagonizes the modification of flot-1 and

cav-1 distribution in lipid rafts brought about by 7βHC (Fig. 6A) while addition of tetracaine alone induces a diffuse distribution of cav-1 in the different gradient fractions. This last result indicates that 7βHC counterbalances the partial inhibition of esterification by tetracaine. This observation is in agreement with the notion that 7βHC activates the ACAT enzyme rather than it inhibits the neutral cholesteryl ester hydrolase [4]. As a consequence, the new equilibrium existing between ACAT inhibition by tetracaine and ACAT activation by the 7βHC delays lipid raft modification and cell death.

Lipid raft play a central role in glucose uptake and on the growth factor cellular functions [40,55]. We have therefore taken a particular interest in the possible impact of the 7βHC-induced modifications of lipid rafts on cell growth, and on the energetic state of the cell. It has been well documented that activation of glucose metabolism is an adaptive response of cancer cells to micro-environmental changes, hypoxia or growth factor deprivation [26]. After 6 h of 7βHC treatment we have observed energy stress and cell growth arrest. Interestingly, AMPK is known, in response to cell stress, to inhibit cholesterol synthesis to decrease metabolic flux through glycolysis and to induce cell cycle arrest, favouring cell survival [27]. Phosphorylation of the ACC enzyme by AMPK results in the inhibition of its catalytic activity transforming acetyl-CoA in malonyl-CoA. Therefore malonyl-CoA synthesis inhibition will reduce lipogenesis and consequently more acetyl-CoA will be available for the Krebs cycle. In accordance with this coupled AMPK/ACC activation we found glucose uptake started to decrease after 8 h while ATP content was maintained by mitochondrial activation (Fig. 4) suggesting a metabolic switch from glycolysis to glucose oxidation. This metabolic switch from glycolysis to glucose oxidation is associated with a shift from cell proliferation to cell growth arrest (Fig. 3B). We concluded that during the first hours following 7βHC treatment, AMPK and mitochondrial activations favour cell survival over cell proliferation.

However, shifting metabolism from glycolysis to glucose oxidation is known to induce apoptosis in glioblastoma [56]. In addition, inhibition of lactate dehydrogenase which promotes the transfer of pyruvate into mitochondria also promotes apoptosis and decreases tumor growth *in vitro* and in mice xenotransplants [57]. We found that subsequent to the phase of increased oxidative phosphorylation, AMPK and ERK are inactivated, the mitochondrial membrane potential is reduced while Akt is activated (Figs. 4 and 5). Activation of the PI3K/Akt pathway has been shown to promote glucose uptake and flux through the early steps of glycolysis [27]. This second cell answer has to be considered as novel attempt to maintain survival and proliferation by increasing glucose metabolism. However, this signaling transition from ERK/AMPK to Akt, coincides with a reduction in glucose uptake and cell lysis (Fig. 3B). This last result indicates that Akt activation as a second response to energy stress is inappropriate. It has previously been shown that GSK3, pAMPK and pERK inhibit mTOR activity and are involved in a cell survival pathway [58–61]. Inactivation of ERK and Akt activation in response to energy stress lead to GSK3β and AMPK inhibition [62] which in their turn lead to mTOR activation and a to deleterious attempt to stimulate proliferation [62–65].

Finally, while Akt activation is reduced after 24 h of 7βHC treatment, P38 reaches its maximum of activation. It is important to notice here that in fetal neural stem cells, activation of mTOR by the notch signaling pathway has been reported to be negatively controlled by a mechanism involving P38 [66]. Notch and mTOR are expressed and functional in C6 [67]. At the same time GSK3 becomes less phosphorylated and therefore more active (Fig. 5). These latter two activations are followed by massive cell death. To further determine the causality between opposing signaling pathway activations and cell death a more detailed time course analysis as well as the use of either kinase inhibitors or isogenic strain mutated on different kinases will be required.

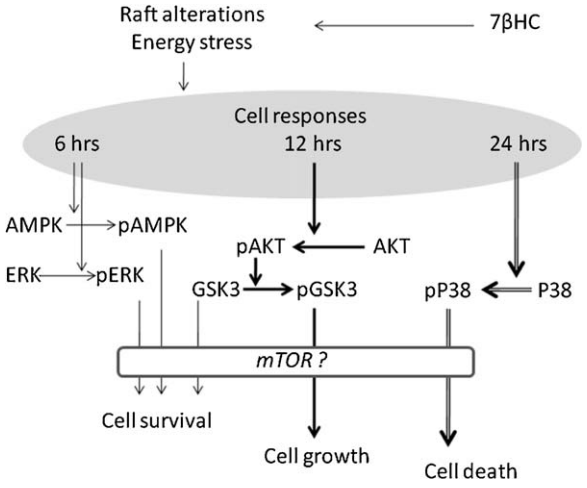

Fig. 7. Sequential opposing signaling responses to 7βHC-induced stress. 7βHC induces lipid-raft sterol and protein modifications and energy stress followed by the sequential activation of AMPK after 6 h (single arrow), Akt after 12 h (bold arrow) and P38 after 24 h (double arrow). ERK and AMPK activate a cell survival pathway, Akt activates an opposing pathway that promotes cell growth and finally P38 leads to cell death by inhibiting the cell growth pathway.

In summary we conclude that three subsequent contradictory cell cycle regulation messages, integrated at the mTOR level to alleviate energy stress by maintaining glucose uptake and intracellular ATP levels end in cell death (Fig. 7). We can also appreciate the relevance of developing drugs, such as 7βHC, to exploit the dependence of tumor cells to maintain glucose consumption.

Acknowledgments

We thank Didier Petite and Clovis Rakotoarivelo for expert technical support, Jean-Philippe Hugnot for scientific exchanges and Gilles Mulin for the interest he gave to this work. This research was supported by l'Agence Nationale de la Recherche (ANR-07-PCVI-0038-01), l'Institut National de la Santé et de la Recherche Médicale (INSERM), L'Ecole Nationale Supérieure de Chimie de Montpellier (ENSCM), and the BetaInnov Company.

References

[1] Giese A, Bjerkvig R, Berens ME, Westphal M. Cost of migration: invasion of malignant gliomas and implications for treatment. J Clin Oncol 2003;21:1624–36.
[2] Werthle M, Bochelen D, Adamczyk M, Kupferberg A, Poulet P, Chambron J, et al. Local administration of 7 beta-hydroxycholesteryl-3-oleate inhibits growth of experimental rat C6 glioblastoma. Cancer Res 1994;54:998–1003.
[3] Kupferberg A, Behr P, Mersel M. Metabolism of 7 beta-hydroxycholesterol in astrocyte primary cultures and derived spontaneously transformed cell lines: correlation between the esterification on C-3-OH by naturally occurring fatty acids and cytotoxicity. Biochim Biophys Acta 1990;1046:106–9.
[4] Behr P, Kupferberg A, Leray C, Schellenbaum L, Urban PF, Vincendon G, et al. Effect of dibutyryl cyclic AMP and isoproterenol on 7 beta-hydroxycholesterol cytotoxicity and esterification in spontaneous transformed cell lines derived from astrocyte primary cultures. FEBS Lett 1992;313:151–4.
[5] Kupferberg A, Teller G, Behr P, Leray C, Urban PF, Vincendon G, et al. Effect of 7 beta-hydroxycholesterol on astrocyte primary cultures and derived spontaneously transformed cell lines: cytotoxicity and metabolism. Biochim Biophys Acta 1989;1013:231–8.
[6] Kupferberg A, Cremel G, Behr P, Van Dorsselaer A, Luu B, Mersel M. Differential sensitivity of astrocyte primary cultures and derived spontaneous transformed cell lines to 7 beta-hydroxycholesterol: effect on plasma membrane lipid composition and fluidity, and on cell surface protein expression. Mol Cell Biochem 1991;101:11–22.
[7] Schroepfer Jr GJ. Oxysterols: modulators of cholesterol metabolism and other processes. Physiol Rev 2000;80:361–554.

[8] Javitt NB. Oxysterols: novel biologic roles for the 21st century. Steroids 2008;73:149–57.
[9] Lea LJ, Hepburn PA, Wolfreys AM, Baldrick P. Safety evaluation of phytosterol esters. Part 8. Lack of genotoxicity and subchronic toxicity with phytosterol oxides. Food Chem Toxicol 2004;42:771–83.
[10] Kandutsch AA, Heiniger HJ, Chen HW. Effects of 25-hydroxycholesterol and 7-ketocholesterol, inhibitors of sterol synthesis, administered orally to mice. Biochim Biophys Acta 1977;486:260–72.
[11] Corcoran RB, Scott MP. Oxysterols stimulate Sonic hedgehog signal transduction and proliferation of medulloblastoma cells. Proc Natl Acad Sci USA 2006;103:8408–13.
[12] Bretillon L, Diczfalusy U, Bjorkhem I, Maire MA, Martine L, Joffre C, et al. Cholesterol-24S-hydroxylase (CYP46A1) is specifically expressed in neurons of the neural retina. Curr Eye Res 2007;32:361–6.
[13] Lizard G, Gueldry S, Sordet O, Monier S, Athias A, Miguet C, et al. Glutathione is implied in the control of 7-ketocholesterol-induced apoptosis, which is associated with radical oxygen species production. FASEB J 1998;12: 1651–63.
[14] Parish EJ, Chitrakorn S, Luu B, Schmidt G, Ourisson G. Studies of the oxysterol inhibition of tumor cell growth. Steroids 1989;53:579–96.
[15] Cheng K, Nagano H, Luu B, Ourisson G, Beck JP. Chemistry and biochemistry of Chinese drugs. Part I. Sterol derivatives cytotoxic to hepatoma cells, isolated from the drug Bombyx cum Botryte. J Chem Res 1977;9:S217.
[16] Moog C, Deloulme JC, Baudier J, Revel MO, Bischoff P, Hietter H, et al. Membrane-related oxysterol function: preliminary results on the modification of protein kinase C activity and substrate phosphorylation by 7 beta, 25-dihydroxycholesterol. Biochimie 1991;73:1321–6.
[17] Hietter H, Bischoff P, Beck JP, Ourisson G, Luu B. Comparative effects of 7 beta-hydroxycholesterol towards murine lymphomas, lymphoblasts and lymphocytes: selective cytotoxicity and blastogenesis inhibition. Cancer Biochem Biophys 1986;9:75–83.
[18] Behr P, Kupferberg A, Leray C, Urban PF, Mersel M. Effect of 7 beta-hydroxycholesterol on astrocyte primary cultures and derived spontaneously transformed cell lines. Cytotoxicity and cholesterogenesis. FEBS Lett 1991;280: 202–6.
[19] Roussi S, Winter A, Gosse F, Werner D, Zhang X, Marchioni E, et al. Different apoptotic mechanisms are involved in the antiproliferative effects of 7beta-hydroxysitosterol and 7beta-hydroxycholesterol in human colon cancer cells. Cell Death Differ 2005;12:128–35.
[20] Heiduschka G, Erovic BM, Vormittag L, Skoda C, Martinek H, Brunner M, et al. 7beta-Hydroxycholesterol induces apoptosis and regulates cyclooxygenase 2 in head and neck squamous cell carcinoma. Arch Otolaryngol Head Neck Surg 2009;135:261–7.
[21] Kang KA, Chae S, Lee KH, Park MT, Lee SJ, Lee YS, et al. Cytotoxic effect of 7beta-hydroxycholesterol on human NCI-H460 lung cancer cells. Biol Pharm Bull 2005;28:1377–80.
[22] Roussi S, Gosse F, Aoude-Werner D, Zhang X, Marchioni E, Geoffroy P, et al. Mitochondrial perturbation, oxidative stress and lysosomal destabilization are involved in 7beta-hydroxysitosterol and 7beta-hydroxycholesterol triggered apoptosis in human colon cancer cells. Apoptosis 2007;12:87–96.
[23] Ryan L, O'Callaghan YC, O'Brien NM. The role of the mitochondria in apoptosis induced by 7beta-hydroxycholesterol and cholesterol-5beta, 6beta-epoxide. Br J Nutr 2005;94:519–25.
[24] Agrawal S, Agarwal ML, Chatterjee-Kishore M, Stark GR, Chisolm GM. Stat1-dependent, p53-independent expression of p21(waf1) modulates oxysterol-induced apoptosis. Mol Cell Biol 2002;22:1981–92.
[25] Miguet C, Monier S, Bettaieb A, Athias A, Bessede G, Laubriet A, et al. Ceramide generation occurring during 7beta-hydroxycholesterol- and 7-ketocholesterol-induced apoptosis is caspase independent and is not required to trigger cell death. Cell Death Differ 2001;8:83–99.
[26] Gatenby RA, Gillies RJ. Why do cancers have high aerobic glycolysis? Nat Rev Cancer 2004;4:891–9.
[27] Vander Heiden MG, Cantley LC, Thompson CB. Understanding the Warburg effect: the metabolic requirements of cell proliferation. Science (New York NY) 2009;324:1029–33.
[28] Iijima T, Mishima T, Akagawa K, Iwao Y. Mitochondrial hyperpolarization after transient oxygen-glucose deprivation and subsequent apoptosis in cultured rat hippocampal neurons. Brain Res 2003;993:140–5.
[29] Palicz A, Foubert TR, Jesaitis AJ, Marodi L, McPhail LC. Phosphatidic acid and diacylglycerol directly activate NADPH oxidase by interacting with enzyme components. J Biol Chem 2001;276:3090–7.
[30] Mosmann T. Rapid colorimetric assay for cellular growth and survival: application to proliferation and cytotoxicity assays. J Immunol Meth 1983;65: 55–63.
[31] Macdonald JL, Pike LJ. A simplified method for the preparation of detergent-free lipid rafts. J Lipid Res 2005;46:1061–7.
[32] Folch J, Lees M, Sloane Stanley GH. A simple method for the isolation and purification of total lipids from animal tissues. J Biol Chem 1957;226:497–509.
[33] Mayor S, Maxfield FR. Insolubility and redistribution of GPI-anchored proteins at the cell surface after detergent treatment. Mol Biol Cell 1995;6: 929–44.
[34] Karu K, Hornshaw M, Woffendin G, Bodin K, Hamberg M, Alvelius G, et al. Liquid chromatography–mass spectrometry utilizing multi-stage fragmentation for the identification of oxysterols. J Lipid Res 2007;48:976–87.
[35] Simons K, Toomre D. Lipid rafts and signal transduction. Nat Rev 2000;1: 31–9.
[36] Smart EJ, Graf GA, McNiven MA, Sessa WC, Engelman JA, Scherer PE, et al. Caveolins, liquid-ordered domains, and signal transduction. Mol Cell Biol 1999;19:7289–304.
[37] Adamczyk M, Scherrer E, Kupferberg A, Malviya AN, Mersel M. Inhibition of p42/p44 mitogen-activated protein kinase by oxysterols in rat astrocyte primary cultures and C6 glioma cell lines. J Neurosci Res 1998;53: 38–50.
[38] Barnes K, Ingram JC, Bennett MD, Stewart GW, Baldwin SA. Methyl-beta-cyclodextrin stimulates glucose uptake in Clone 9 cells: a possible role for lipid rafts. Biochem J 2004;378:343–51.
[39] Neumann-Giesen C, Fernow I, Amaddii M, Tikkanen R. Role of EGF-induced tyrosine phosphorylation of reggie-1/flotillin-2 in cell spreading and signaling to the actin cytoskeleton. J Cell Sci 2007;120:395–406.
[40] Freeman MR, Cinar B, Kim J, Mukhopadhyay NK, Di Vizio D, Adam RM, et al. Transit of hormonal and EGF receptor-dependent signals through cholesterol-rich membranes. Steroids 2007;72:210–7.
[41] Kahn BB, Alquier T, Carling D, Hardie DG. AMP-activated protein kinase: ancient energy gauge provides clues to modern understanding of metabolism. Cell Metab 2005;1:15–25.
[42] Hardie DG, Carling D. The AMP-activated protein kinase—fuel gauge of the mammalian cell? Eur J Biochem/FEBS 1997;246:259–73.
[43] Park H, Kaushik VK, Constant S, Prentki M, Przybytkowski E, Ruderman NB, et al. Coordinate regulation of malonyl-CoA decarboxylase, sn-glycerol-3-phosphate acyltransferase, and acetyl-CoA carboxylase by AMP-activated protein kinase in rat tissues in response to exercise. J Biol Chem 2002;277: 32571–7.
[44] Bandyopadhyay G, Sajan MP, Kanoh Y, Standaert ML, Burke Jr TR, Quon MJ, et al. Glucose activates mitogen-activated protein kinase (extracellular signal-regulated kinase) through proline-rich tyrosine kinase-2 and the Glut1 glucose transporter. J Biol Chem 2000;275:40817–26.
[45] Briaud I, Lingohr MK, Dickson LM, Wrede CE, Rhodes CJ. Differential activation mechanisms of Erk-1/2 and p70(S6K) by glucose in pancreatic beta-cells. Diabetes 2003;52:974–83.
[46] Fecchi K, Volonte D, Hezel MP, Schmeck K, Galbiati F. Spatial and temporal regulation of GLUT4 translocation by flotillin-1 and caveolin-3 in skeletal muscle cells. FASEB J 2006;20:705–7.
[47] Xi X, Han J, Zhang JZ. Stimulation of glucose transport by AMP-activated protein kinase via activation of p38 mitogen-activated protein kinase. J Biol Chem 2001;276:41029–34.
[48] Uittenbogaard A, Ying Y, Smart EJ. Characterization of a cytosolic heat-shock protein-caveolin chaperone complex. Involvement in cholesterol trafficking. J Biol Chem 1998;273:6525–32.
[49] Salzer U, Prohaska R. Stomatin, flotillin-1, and flotillin-2 are major integral proteins of erythrocyte lipid rafts. Blood 2001;97:1141–3.
[50] Murata M, Peranen J, Schreiner R, Wieland F, Kurzchalia TV, Simons K. VIP21/caveolin is a cholesterol-binding protein. Proc Natl Acad Sci USA 1995;92: 10339–43.
[51] Sleer LS, Brown AJ, Stanley KK. Interaction of caveolin with 7-ketocholesterol. Atherosclerosis 2001;159:49–55.
[52] Uittenbogaard A, Everson WV, Matveev SV, Smart EJ. Cholesteryl ester is transported from caveolae to internal membranes as part of a caveolin–annexin II lipid–protein complex. J Biol Chem 2002;277:4925–31.
[53] Le Lay S, Li Q, Proschogo N, Rodriguez M, Gunaratnam K, Cartland S, et al. Caveolin-1-dependent and -independent membrane domains. J Lipid Res 2009;50:1609–20.
[54] Podar K, Tai YT, Cole CE, Hideshima T, Sattler M, Hamblin A, et al. Essential role of caveolae in interleukin-6- and insulin-like growth factor I-triggered Akt-1-mediated survival of multiple myeloma cells. J Biol Chem 2003;278: 5794–801.
[55] Sanchez-Wandelmer J, Davalos A, Herrera E, Giera M, Cano S, de la Pena G, et al. Inhibition of cholesterol biosynthesis disrupts lipid raft/caveolae and affects insulin receptor activation in 3T3-L1 preadipocytes. Biochim Biophys Acta 2009;1788:1731–9.
[56] Michelakis ED, Sutendra G, Dromparis P, Webster L, Haromy A, Niven E. Metabolic modulation of glioblastoma with dichloroacetate. Sci Transl Med 2010;2:31.ra4.
[57] Fantin VR, St-Pierre J, Leder P. Attenuation of LDH-A expression uncovers a link between glycolysis, mitochondrial physiology, and tumor maintenance. Cancer Cell 2006;9:425–34.
[58] Corradetti MN, Inoki K, Bardeesy N, DePinho RA, Guan KL. Regulation of the TSC pathway by LKB1: evidence of a molecular link between tuberous sclerosis complex and Peutz–Jeghers syndrome. Genes Dev 2004;18:1533–8.
[59] Shaw RJ, Bardeesy N, Manning BD, Lopez L, Kosmatka M, DePinho RA, et al. The LKB1 tumor suppressor negatively regulates mTOR signaling. Cancer Cell 2004;6:91–9.
[60] Brugarolas J, Lei K, Hurley RL, Manning BD, Reiling JH, Hafen E, et al. Regulation of mTOR function in response to hypoxia by REDD1 and the TSC1/TSC2 tumor suppressor complex. Genes Dev 2004;18:2893–904.
[61] Inoki K, Ouyang H, Zhu T, Lindvall C, Wang Y, Zhang X, et al. TSC2 integrates Wnt and energy signals via a coordinated phosphorylation by AMPK and GSK3 to regulate cell growth. Cell 2006;126:955–68.
[62] Hahn-Windgassen A, Nogueira V, Chen CC, Skeen JE, Sonenberg N, Hay N. Akt activates the mammalian target of rapamycin by regulating cellular ATP level and AMPK activity. J Biol Chem 2005;280:32081–9.
[63] Inoki K, Zhu T, Guan KL. TSC2 mediates cellular energy response to control cell growth and survival. Cell 2003;115:577–90.

[64] Inoki K, Ouyang H, Li Y, Guan KL. Signaling by target of rapamycin proteins in cell growth control. Microbiol Mol Biol Rev 2005;69:79–100.
[65] Ma L, Chen Z, Erdjument-Bromage H, Tempst P, Pandolfi PP. Phosphorylation and functional inactivation of TSC2 by Erk implications for tuberous sclerosis and cancer pathogenesis. Cell 2005;121:179–93.
[66] Androutsellis-Theotokis A, Leker RR, Soldner F, Hoeppner DJ, Ravin R, Poser SW, et al. Notch signalling regulates stem cell numbers in vitro and in vivo. Nature 2006;442:823–6.
[67] Cobelens PM, Kavelaars A, Heijnen CJ, Ribas C, Mayor Jr F, Penela P. Hydrogen peroxide impairs GRK2 translation via a calpain-dependent and cdk1-mediated pathway. Cell Signal 2007;19:269–77.
[68] Bochelen D, Eclancher F, Kupferberg A, Privat A, Mersel M. 7 beta-Hydroxycholesterol and 7 beta-hydroxycholesteryl-3-esters reduce the extent of reactive gliosis caused by an electrolytic lesion in rat brain. Neuroscience 1992;51:827–34.